Available online at www.sciencedirect.com
ScienceDirect
Acta Materialia 55 (2007) 897–905
Acta MATERIALIA
www.actamat-journals.com

The role of twinning and untwinning in yielding behavior in hot-extruded Mg–Al–Zn alloy

Y.N. Wang [a,b], J.C. Huang [a,*]

[a] Institute of Materials Science and Engineering, Center for Nanoscience and Nanotechnology, National Sun Yat-Sen University, Kaohsiung 804, Taiwan

[b] Institute of Materials Science and Engineering, Dalian University of Technology, Dalian 116024, China

Received 28 July 2006; received in revised form 12 September 2006; accepted 14 September 2006
Available online 29 November 2006

Abstract

This paper examines the effect of compressive pre-deformation on subsequent tensile deformation behavior in a hot-extruded AZ31 Mg alloy bar with a ring fiber texture, and with the basal planes parallel to the extrusion direction. Such an orientation favors extensive $\{10\bar{1}2\}$ twinning under compressive loading, resulting in a comparably low compressive yield stress. In contrast, the basal slip and $\{10\bar{1}2\}$ twinning are difficult to operate under tensile testing, resulting in a high tensile yield strength. Compressive pre-deformation causes a significant drop in tensile yield strength, from ~265 to ~160 MPa, irrespective of the amount of pre-deformation strain. The latter value of ~160 MPa nearly coincides with the compressive yield strength. The lattice reorientation of 86.3° caused by twinning during compressive loading favors untwinning in the twinned areas during subsequent tensile reloading, leading to a significant drop in tensile yield strength.

Keywords: Magnesium alloy; Extrusion; Twinning; Yield phenomena

1. Introduction

The application of magnesium alloys for lightweight structural components has significantly increased during the last decade, mainly due to the rapid expansion of high-pressure die casting components in the electronic and automotive industries. However, casting defects, such as porosity and inclusions, as well as the rather low ductility of many cast alloys, restrict the wide use of common cast magnesium alloy components. Although wrought alloys are known to offer generally better mechanical properties than cast alloys, structural applications of magnesium alloys processed by extrusion, forging or rolling are still very scarce. The major problems encountered in wrought components are the poor workability and the strong directionality of properties, which are caused by the particular deformation characteristics of the hexagonal crystal structure.

It has long been understood that the limited formability of magnesium and its alloys at room temperature is attributed to the highly anisotropic dislocation slip behavior. Critical resolved shear stresses (CRSS) have already been reported for three different slip systems in single crystal magnesium [1,2]. According to the reported data, the CRSS for a basal slip system of $1/3\langle 11\bar{2}0\rangle$ or $\langle a\rangle$ type dislocations at room temperature is much lower than those of the non-basal slip systems on prismatic and pyramidal planes, as well as the twinning modes. Therefore, plastic deformation in polycrystalline alloys appears to occur almost entirely by basal slip. Because the basal slip systems provide only two independent slip systems, far fewer than the necessary five independent systems for homogeneous deformation, the limited slip systems will result in poor formability. Simultaneously, the limited

* Corresponding author. Tel.: +886 7 5252000x4063; fax: +886 7 5254099.
E-mail address: jacobc@mail.nsysu.edu.tw (J.C. Huang).

1359-6454/$30.00
doi:10.1016/j.actamat.2006.09.010

number of active deformation systems in hexagonal close-packed (hcp) metals results in the formation of a strong crystallographic texture upon mechanical processing. The anisotropy of mechanical properties is due mainly to a pronounced texture. As a result, when the wrought magnesium alloys have a strong crystallographic texture that develops during plastic deformation, their mechanical properties are significantly influenced by the crystallographic textures in addition to other effects, such as grain size or precipitations [3–9]. The grain size dependence of the mechanical properties in magnesium and its alloys was specifically addressed in detail by Armstrong and Zerilli [10].

Previous reports indicate that some cast alloys also exhibit reasonable ductility, with a tensile elongation of more than 10% at room temperature. More recently, Yamashita et al. [11] reported that elongation-to-failure of the AZ31 Mg alloy was improved by up to ~15% when the grain size was reduced from ~100 to ~20 μm. Furthermore, this alloy, when subjected to equal channel angular pressing, exhibited a tensile elongation of more than 40% at room temperature when grain size was further reduced to ~1 μm [12]. Such large elongation values cannot be contributed solely by the basal slip system mechanism of plastic deformation.

It is also recognized that the incorporation of non-basal slip of ⟨a⟩ dislocations on the prismatic $\{10\bar{1}0\}$ or even the fist-order pyramidal $\{10\bar{1}1\}$ planes offers only two more independent slip modes. Additionally, the presence of mechanical twinning modes further improves the situation by essentially offering another independent mode of deformation.

It is well known that twinning deformation modes play an important role during the deformation of hexagonal magnesium. Despite the limited contribution of twinning itself to the total plasticity (the twinning shear is only about 0.13; cf. Section 2), the abrupt change of orientation due to twinning may give rise to the reactivation of other slip systems. For metals with a c/a ratio (where a and c are the lattice constants in hexagonal lattices) of less than $\sqrt{3}$ (e.g. titanium, zirconium, and magnesium), normally only the $\{10\bar{1}2\}\langle 10\bar{1}1\rangle$ twin is activated by c-axis tension. During compression, grains are favorably oriented if their c-axis is perpendicular to the compression axis; and the twinning reorients the c-axis of the twin nearly parallel to the compression axis.

Much work has been carried out to establish the relationship between initial orientation and deformation mechanisms [13–17]. However, detailed information about the influence of twinning on the tensile plastic deformation and texture formation is relatively limited. The study reported in the present paper was carried out to investigate the influence of compressive pre-deformation on subsequent tensile plastic deformation in a hot-extruded AZ31 alloy bar with a near-ring $\{0002\}$ fiber texture. The change of orientation due to twinning on the reactivation of slip during tensile deformation is analyzed.

2. Deformation twinning in magnesium lattice

Materials with hcp lattices exhibit many types of twinning. However, for all hexagonal metals at low homologous temperatures, deformation twinning on $\{01\bar{1}2\}$ planes is the dominant mechanism, which allows for inelastic shape changes in the c-axis. The full description of the $\{10\bar{1}2\}$ deformation twinning mode is [18,19]:

$$K_1 = \{10\bar{1}2\},\ K_2 = \{\bar{1}012\},\ \eta_1 = \langle\bar{1}011\rangle,\ \eta_2 = \langle\bar{1}01\bar{1}\rangle \quad (1)$$

$$\gamma_0 = \frac{\sqrt{3}}{(c/a)} - \frac{(c/a)}{\sqrt{3}} \quad (2)$$

where K_1, K_2, η_1, and η_2 have their usual meanings in twinning designation. The amount of shear γ_0 associated with twinning depends on the c/a ratio. Such a twinning system is shown schematically in Fig. 1. For the materials with $c/a < \sqrt{3}$, the direction of shear is $[\bar{1}011]$, and the twinning occurs under tension parallel to the c-axis or under compression perpendicular to the c-axis. In magnesium

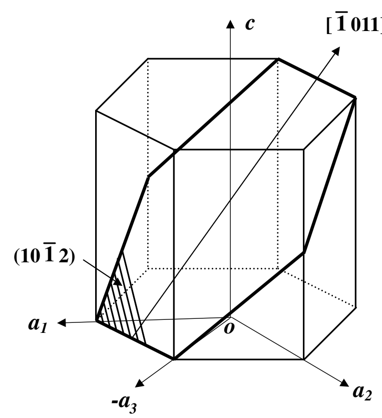

Fig. 1. The $\{10\bar{1}2\}\langle\bar{1}011\rangle$ tensile twinning system for the hcp-Mg metal.

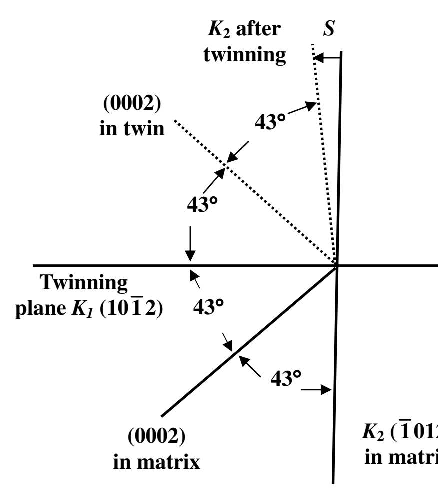

Fig. 2. Shear sense for $\{10\bar{1}2\}$ twinning in the hcp-Mg metal (c/a = 1.624). Symmetry conditions require that the second undistorted plane, K_2, be rotated counterclockwise in magnesium. This has the effect of shortening the crystal inside the twinned volume in a direction parallel to the basal plane.

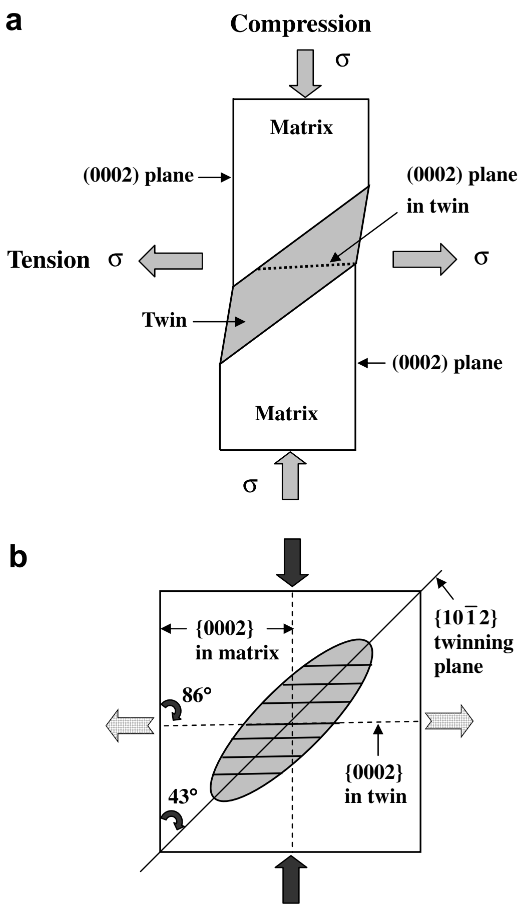

Fig. 3. The formation of a $\{10\bar{1}2\}$ twin in the hcp-Mg metal decreases the length of the crystal in a direction parallel to the basal plane, indicating that twinning is favored by a compressive stress applied parallel to the basal plane or a tensile stress applied perpendicular to the basal plane. (a) Deformation sense for $\{10\bar{1}2\}$ twinning; (b) geometry relationship between the matrix and twin.

and its alloys, the c/a ratio is ~1.624, the twinning shear is 0.1289 according to Eq. (2), and there is a 43.15° angle between the basal $\{0002\}$ plane and the twinning $\{10\bar{1}2\}$ planes. Because symmetry conditions require that the second undistorted plane, K_2, be rotated counterclockwise in magnesium lattice, this has the effect of shortening the crystal inside the twinned volume in a direction parallel to the basal plane, as shown in Fig. 2. This is why the twinning occurs under tension parallel to the c-axis or under compression perpendicular to the c-axis. The formation of $\{10\bar{1}2\}$ twin in magnesium lattices decreases the length of the crystal in a direction parallel to the basal plane. A compressive stress applied parallel to the basal plane or a tensile stress applied perpendicular to the basal plane will twin in a magnesium crystal, as shown in Fig. 3. Also, an early and updated description for twinning and untwinning in magnesium crystals can be referred elsewhere [20,21].

3. Experimental methods

The as-received AZ31B billet used in this study were obtained from the CDA Company, Delta, BC, Canada. The chemical composition is Mg–3.02% Al–1.01% Zn–0.30% Mn (in mass%). This alloy is a solution-hardened alloy with minimum precipitation. The as-received billet possessed nearly equiaxed grains around 75 μm. Extrusion was conducted at a container temperature of 400 °C with an extrusion ratio of 42:1, resulting in a rod measuring 10 mm in diameter.

The round compressive specimens (12 mm in height and 7 mm in diameter) and tensile specimens (10 mm gage length and 3 mm gage diameter) were prepared using electrical-discharge machining from the extruded rod. Both the compressive and tensile directions were aligned parallel to the extrusion direction. Compressive and tensile tests were conducted using an Instron-5582 universal testing machine with an initial strain rate of $1 \times 10^{-3}\,s^{-1}$ at room temperature.

In order to evaluate the textures generated by hot extrusion, the $\{0002\}$, $\{10\bar{1}0\}$, and $\{10\bar{1}1\}$ pole figures were measured by the Schulz reflection method using a Dede-D1 X-ray diffractometer to observe the transverse cross-sectional plane, using Cu Kα radiation (wave length $\lambda = 0.15406$ nm) at 40 kV and 200 mA with a sample tilt angle ranging from 0 to 85°. The grain structures of all samples were examined by optical microscopy (OM). The grain size was analyzed by the Optimas image software on OM photographs at different magnifications.

4. Results

4.1. Initial state

The microstructure of the as-extruded AZ31 alloy is shown in Fig. 4. It consists of fine and equiaxed grains with a mean grain size of about 5 μm. Fig. 5 shows the experimental pole figures of the extruded AZ31 rod with its reflecting surface normal to the extrusion direction.

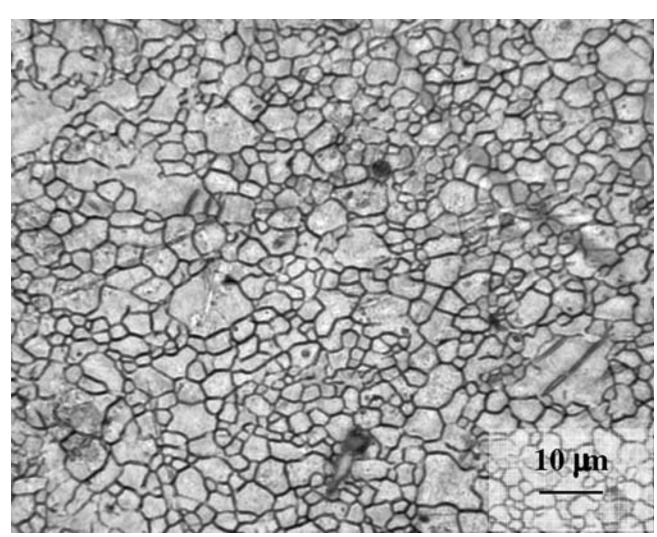

Fig. 4. The microstructure seen from the cross-sectional plane of the as-extruded AZ31 bar.

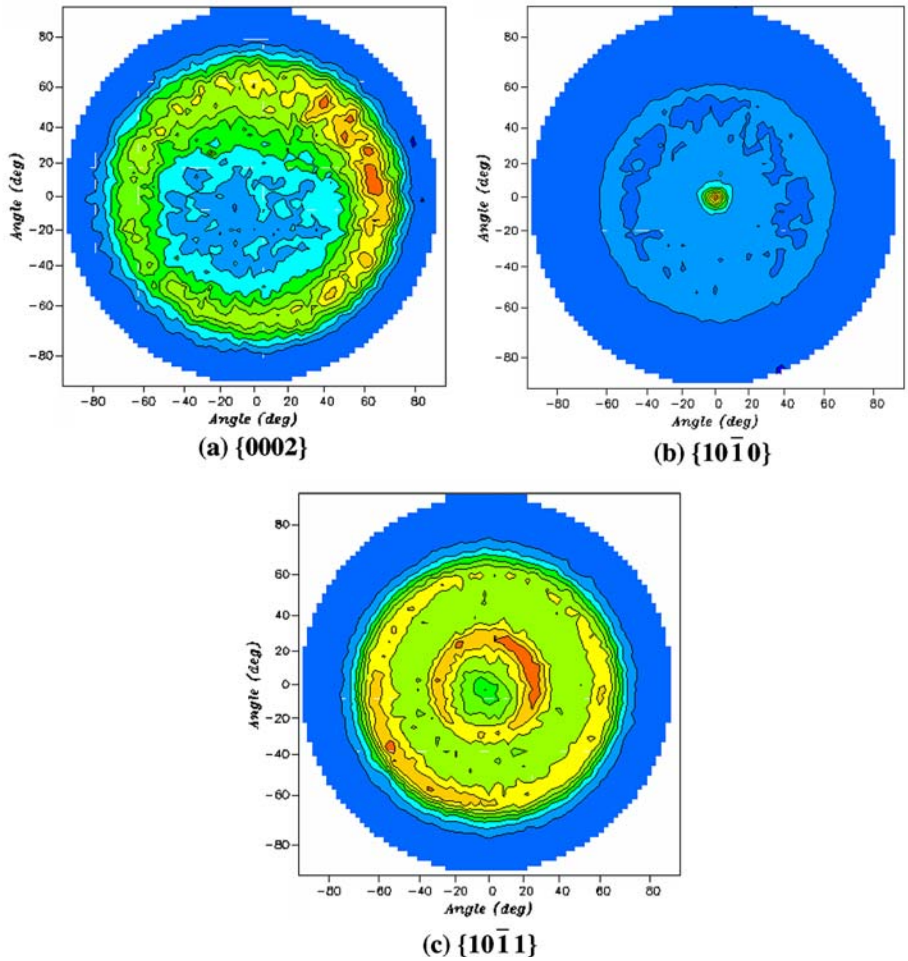

Fig. 5. Experimental pole figures of the as-extruded AZ31 bar, showing a nearly ring fiber texture with the basal planes parallel to the extrusion direction.

According to the prismatic $\{10\bar{1}0\}$ pole figure, the $\{10\bar{1}0\}$ plane is strictly parallel to the extrusion direction. And according to pyramidal $\{10\bar{1}1\}$ pole figure, the $\{10\bar{1}1\}$ planes are nearly homogeneously distributed, with tilting of ~27 and ~63° round the extrusion direction, which corresponds to the nearly homogeneous distribution of the $\{0002\}$ basal plane parallel to the extrusion direction. Thus, the texture can be roughly considered as having a ring fiber texture with the basal planes parallel to the extrusion direction with a spread of around 10°.

4.2. Compressive plastic deformation

A typical compressive stress–strain curve of the extruded AZ31 sample loaded parallel to extrusion direction is shown in Fig. 6. The compressive yield stress (YS) and the ultimate compressive strength (UCS) are ~160 and ~370 MPa, as listed in Table 1. Remarkably, the present compressive curve exhibited a low yield stress and a clear yielding plateau, namely, low work hardening at low strains and a subsequent gradual increase of the hardening until close to the peak stress and fracture. The curve did not reveal a peak-type flow curve, obviously due to homogeneous deformation. This is confirmed by the microstructure of the samples deformed to ~3% strain and to failure (~15% thickness reduction), as shown in Fig. 7a and b. No evident crack but a large number of deformation twins were found in both of the compressively deformed samples.

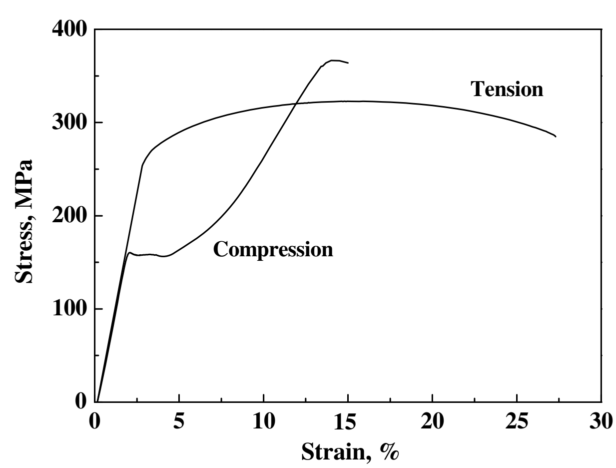

Fig. 6. Typical engineering compressive and tensile stress–strain curves of the as-extruded AZ31 samples loaded parallel to the extrusion direction.

Table 1
Compressive and tensile properties of the extruded AZ31 bar

Loading mode	Pre-compression	YS (MPa)	US (MPa)	δ (%)
Compression	–	∼160	∼370	∼15
Tension	–	∼265	∼320	∼28
Compression then tension	∼1%	∼160	∼345	∼28
Compression then tension	∼3%	∼160	∼350	∼27

YS, 0.2% yield stress; US, ultimate compressive or tensile strength; δ, strain to failure.

X-ray diffraction (XRD) scans of the extruded AZ31 samples after compressive deformation are shown in Fig. 8a. It can be clearly seen that the XRD intensity of the (0002) peak (denoted as $I_{(0002)}/I_{(10-10)}$ ratio) increased significantly from ∼0.25 before compressive deformation up to ∼6 after ∼3% strain compressive deformation. This suggests that the abrupt change of orientation due to twinning can occur at a low degree of compressive deformation. Also, the new orientation is quite stable until fracture. It is reasonable to suggest that an increase in the intensity of the (0002) peak is directly related to the twinning and basal slip deformation mechanisms.

4.3. Tensile plastic deformation

A typical tensile stress–strain curve of the extruded AZ31 sample loaded parallel to extrusion direction is included in Fig. 6. The tensile yield stress and the ultimate tensile strength (UTS) are ∼265 and ∼320 MPa, as listed in Table 1. The present tensile curve exhibited a higher yielding stress, and subsequently low work hardening until close to the peak stress and necking fracture. Compared with the compressive curve, it can be deduced that different deformation behaviors have taken place during compressive and tensile deformation. The microstructures of the tensile samples deformed to ∼3% strain and to failure (∼30%), shown in Fig. 7c and d, indicate that no evident twinning was found in the tensile deformed samples. It is also confirmed by XRD that the intensity of the (0002) peak shows little change before and after tensile deformation, with no evident change of orientations, as illustrated in Fig. 8b.

4.4. Effect of compressive pre-deformation on tensile plastic deformation

The effect of compressive pre-deformation on the stress–strain curve of the extruded AZ31 alloy during subsequent reloading of tension is illustrated in Fig. 9. It can be seen that the compressive pre-deformation causes a significant

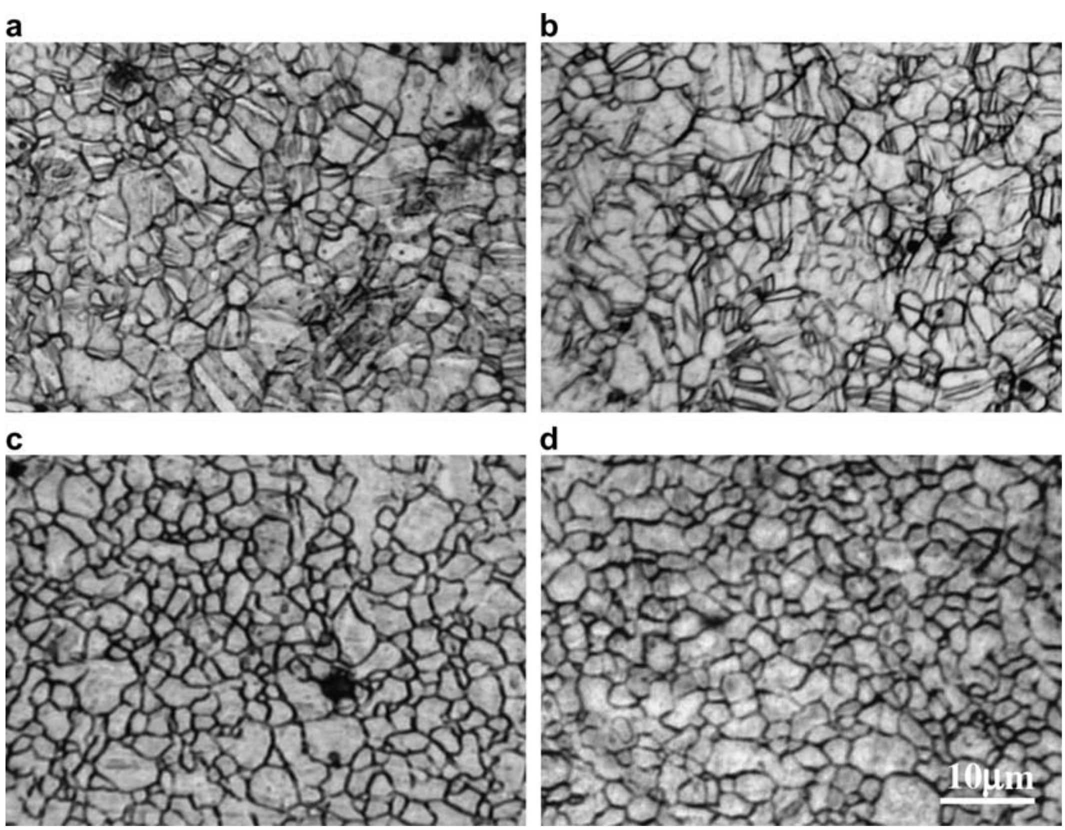

Fig. 7. Microstructures seen from the cross-sectional plane of the extruded samples deformed under compression to (a) ∼3% strain and (b) failure (∼15% thickness reduction), showing intense twinning, and seen from the samples deformed under tension to (c) ∼3% strain and (d) failure (∼30%), showing no evidence of twinning.

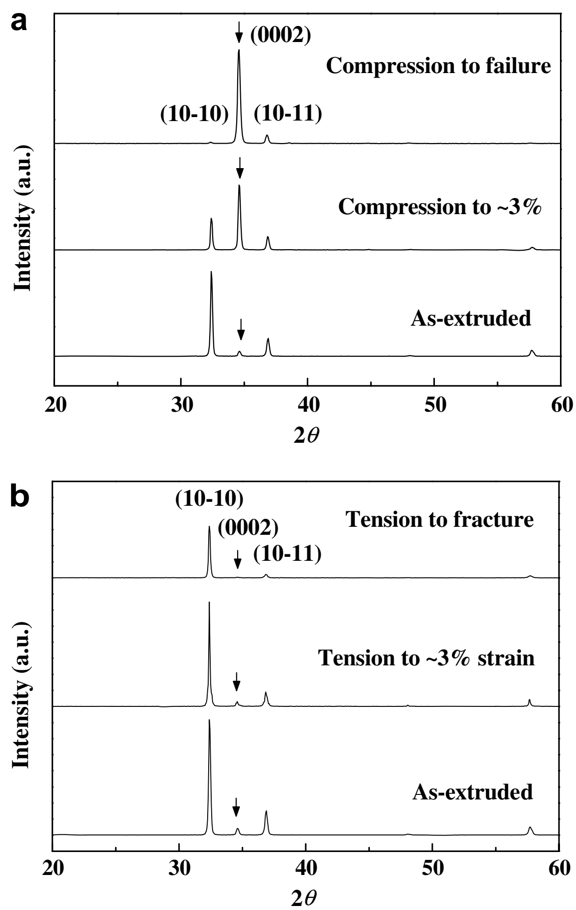

Fig. 8. XRD scans from the cross-sectional planes of the as-extruded AZ31 samples: (a) after compressive deformation to different strains, showing obvious changes of orientations; and (b) after tensile deformation to different strains, showing no evident change of orientation.

drop in tensile yield stress, from ~265 to ~160 MPa, irrespective of the amount of compression pre-strain. The latter value, ~160 MPa, nearly coincides with the compressive yield stress. This suggests that the tensile yielding behavior for the compressively pre-deformed samples is similar to the compressive yielding behavior for the sample without pre-deformation. The tensile properties of the samples with and without pre-deformation are included in Table 1. In comparison with the strain value of the pre-deformed samples at the stress level of ~265 MPa, it can be seen that the strain intervals from YS to $\sigma = 265$ MPa for the 1% and 3% pre-deformed specimens correlate well with the pre-strained amount (cf. Fig. 9), suggesting that the strain caused by twinning during compressive pre-deformation might be recovered by untwinning during subsequent tensile deformation. This is also confirmed by the XRD scans from the cross-sectional planes of the pre-compressed samples and subjected to subsequent tension to ~3% strain and to failure, as shown in Fig. 10. It can be seen that the obvious changes of orientations in term of the (0002) peaks occurred during subsequent tensile deformation owing to the untwinning process.

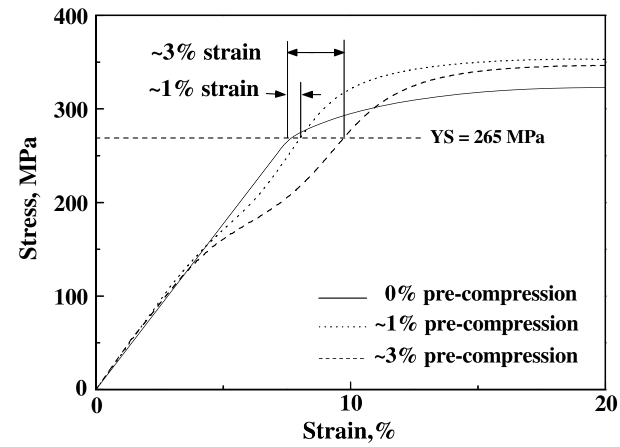

Fig. 9. Typical tensile flow curves of the tensile-loaded AZ31 samples with and without pre-compression deformation.

4.5. Schmid factor for twinning

The Schmid facor for twinning is defined as:

$$M_{tw} = \cos\chi_{tw} \cdot \cos\lambda_{tw} \tag{3}$$

where χ_{tw} is the angle between the normal to $\{10\bar{1}2\}$ twinning plane and the stress axis, and λ_{tw} is the angle between the direction of shear and the stress axis [22]. The hcp crystal lattice of magnesium features the six equivalent twinning planes and the Schmid factors for these twinning systems can be calculated numerically for any possible orientation of the grain in the textured polycrystalline alloy. In the present paper, the system with the highest Schmid factor is supposed to become activated in any grain and multiple twinning is not considered here.

For the present ring fiber texture, the χ angle changes from 53 to 46°, and the λ angle changes from 50 to 44° over all possible grain orientations, as shown in Fig. 11. Thus, the average Schmid factor is written as

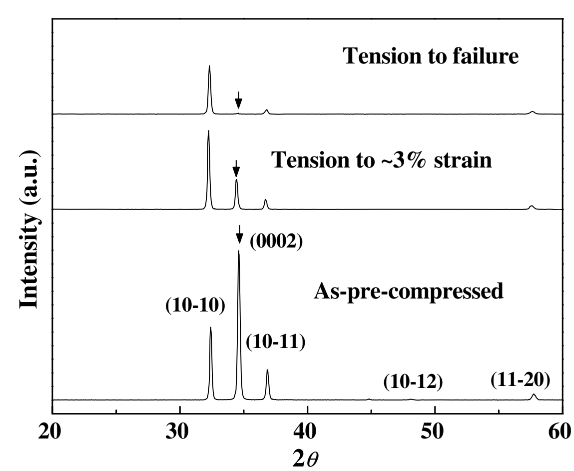

Fig. 10. XRD scans from the cross-sectional planes of the as-pre-compressed AZ31 samples and the specimens subjected to subsequent tension to ~3% strain and to failure, showing obvious changes of orientations owing to the untwinning process.

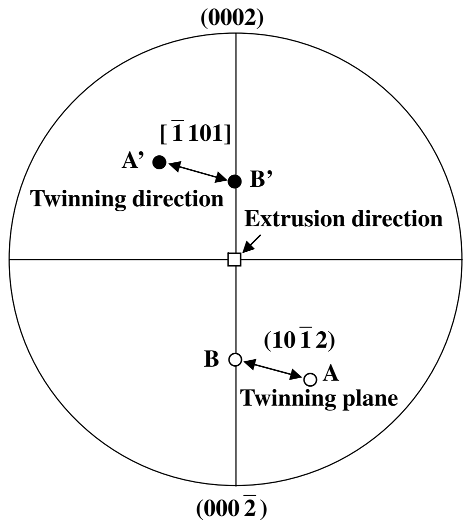

Fig. 11. Schematic drawing showing the changes of the twinning plane and twinning direction over all possible grain orientations of the ring fiber texture in the hcp-Mg metal when the loading axis is aligned parallel to the extrusion direction. The range of the twinning plane changes from position A to B, and the range of the corresponding twinning direction changes from position A′ to B′.

$$\overline{M}_{\mathrm{tw}} = \frac{1}{n}\sum_{i=1}^{n} \cos\chi_i \cos\lambda_i \tag{4}$$

For the sake of simplicity, two cases are taken into account. When the stress axis is parallel to the $[11\bar{2}0]$ direction, χ is $\sim$53° and λ is $\sim$50°, then the Schmid factor for twinning is $M_{\mathrm{tw}} = \cos\chi\cos\lambda = 0.602 \times 0.643 = 0.387$. When stress axis is parallel to $[10\bar{1}0]$ direction, the optimal χ is $\sim$46° and the optimal λ is $\sim$44°, then the Schmid factor for twinning is $M_{\mathrm{tw}} = \cos\chi\cos\lambda = 0.695 \times 0.719 = 0.499$. Thus, the average Schmid factor for twinning can be calculated roughly to be $\overline{M}_{\mathrm{tw}} = (0.387 + 0.499)/2 = 0.443$ for the present ring fiber texture.

5. Discussion

5.1. Compressive deformation behavior

In principle, hexagonal materials can deform by crystallographic slip and deformation twinning. Crystallographic slip is liable to occur in basal slip system $\{0002\}\langle 11\bar{2}0\rangle$, prismatic slip system $\{10\bar{1}0\}\langle 11\bar{2}0\rangle$, and pyramidal slip systems $\{10\bar{1}1\}\langle 11\bar{2}0\rangle$, $\{10\bar{1}2\}\langle 11\bar{2}0\rangle$ or $\{11\bar{1}2\}\langle 11\bar{2}3\rangle$. It is noted that the latter slip system has a slip direction not parallel to the basal plane, known as the $\langle \boldsymbol{c}+\boldsymbol{a}\rangle$-Burgers vector. While there are several potential twinning systems, only the $\{10\bar{1}2\}\langle 10\bar{1}1\rangle$ system is often observed in most hcp metals, particularly in magnesium. As mentioned in Section 2, this twinning system is the so-called "tension twin" in magnesium, since it can only be activated by a tensile stress parallel to the c-axis (perpendicular to the basal plane) when the c/a is less than $\sqrt{3}$.

The present hot-extruded sample provided an initial texture where the sample orientation does not allow any twinning under tensile loading but maximum twinning under compressive loading. Therefore, this starting texture could activate the $\{10\bar{1}2\}\langle 10\bar{1}1\rangle$ twinning at a low degree of deformation, and could result in a comparably low yield stress. Due to the activity of twinning, the c-axis of twin in the compressively deformed samples would orient nearly parallel to the compression axis. At a low degree of compressive deformation, the microstructure would be dominated by intense twinning, as shown in Fig. 7a and b. The abrupt change of orientation due to twinning was also confirmed by XDR scans, which showed that the intensity of the (0002) peak extremely increased from $\sim$0.25 before compressive deformation up to $\sim$6 after 3% compressive deformation, as shown in Fig. 8a.

For the present sample orientation, the basal slip is limited for both compressive and tensile loading conditions due to the small orientation factor, which denotes a very low shear stress on the basal slip system. However, the CRSS for basal slip is very low, $\sim$0.5 MPa in pure magnesium and $\sim$2 MPa in AZ31 alloy. A slight misalignment ($\pm$10°) of the basal plane can thus lead to the operation of this slip mode, so the activation of basal slip in the present sample is still likely.

On the other hand it has recently been shown that a CRSS criterion is also reasonable for $\{10\bar{1}2\}$ twinning and the CRSS for an Mg–7.7 at.% Al (or Mg–8.5 wt.% Al) alloy free of precipitates was determined to be 65–75 MPa [23]. The current softer AZ31 alloy contains only 3 wt.% Al, and the CRSS for $\{10\bar{1}2\}$ twinning might be around 40–50 MPa. Since most grains are very favorably oriented for $\{10\bar{1}2\}$ twinning in compression, the compressive yield stress, σ_{ys}, can be roughly estimated to be $\sim$100 MPa according to the following equation, if neglecting the influence of grain size:

$$\sigma_{\mathrm{ys}} = \tau_{CRSS(tw)}/M_{\mathrm{tw}} \tag{5}$$

where τ_{CRSS} of 40–50 MPa is the CRSS for twinning; M_{tw} of $\sim$0.443 (see Section 4.5) is the orientation or Schmid factor for twinning. The measured compressive yield stress of $\sim$160 MPa seems to include the major contribution from twinning, plus minor grain size strengthening.

The present compressive stress–strain curve exhibits a clear yielding plateau and the subsequent gradual increase of the hardening until close to the fracture, as shown in Fig. 6. From the analysis of the deformation mechanisms and the observed microstructures, this compressive deformation behavior has to be contributed by extensive twinning at low strains. Obviously, twinning can be activated at a relatively low stress, and massive twinning will lead to a low strain hardening rate. Only when the twinning capacity is exhausted due to the formation of basal texture will a strong strain hardening due to the slip and slip–twinning interaction be achieved. This complicated deformation experience leads to massive shear band formation and cracking once slip and twinning cannot accommodate the shape change any more, whereupon fracture will take place. The complicated interaction between extensive twinning and slip at the later compressive straining stage, causing a fast increment of work hardening, will restrict further plastic deformation and induce premature local cracking. It follows that the compressive failure strain (∼15%) is appreciably lower than the tensile failure strain (∼28%) of the current fine grained AZ31 Mg alloy.

5.2. Tensile deformation behavior

As mentioned above, the present initial texture does not favor any basal slip and twinning for tensile loading. However, because the CRSS for basal slip is very low (∼2 MPa) in the AZ31 alloy, some grains with a random texture and a slight misalignment (±10°) of the basal plane can lead to the operation of the basal slip mode. Thus, the tensile plastic deformation in the early stage will be dominated by basal slip. It is expected that the tensile yield stress is reasonable higher (∼265 MPa), owing to the low Schmid factor for slip compared with the compressive yield stress (∼160 MPa) when loading is applied along the extrusion direction.

However, as is obvious from the tensile deformation characteristic and texture development, the deformation mode was strongly affected by compressive pre-deformation. Since $\{10\bar{1}2\}$ twinning leads to a reorientation of 86.3° of the crystal lattice, all the basal planes in twinned lattices lie nearly perpendicular to the extrusion direction after compressive plastic deformation, as shown in Fig. 12. These twinned regions are capable of untwinning during reloading in subsequent tension. This is indeed what can be observed in Fig. 9. After the onset of twinning at a yield stress of about ∼160 MPa, the curvature becomes convex, which is typical for deformation by twinning. From the differences in strain between the curves in Fig. 9, it can be concluded that all the strains caused by twinning during compressive pre-deformation can be recovered by untwinning during subsequent early tensile deformation, which results in the convex nature of the curvature. Similar to the compressive stress–strain curve, the tensile stress–strain curves for the compressively pre-deformed samples also exhibit low yield stress at low strains, and a subsequent pronounced increase of the hardening rate until close to the peak strain. The yield stress is

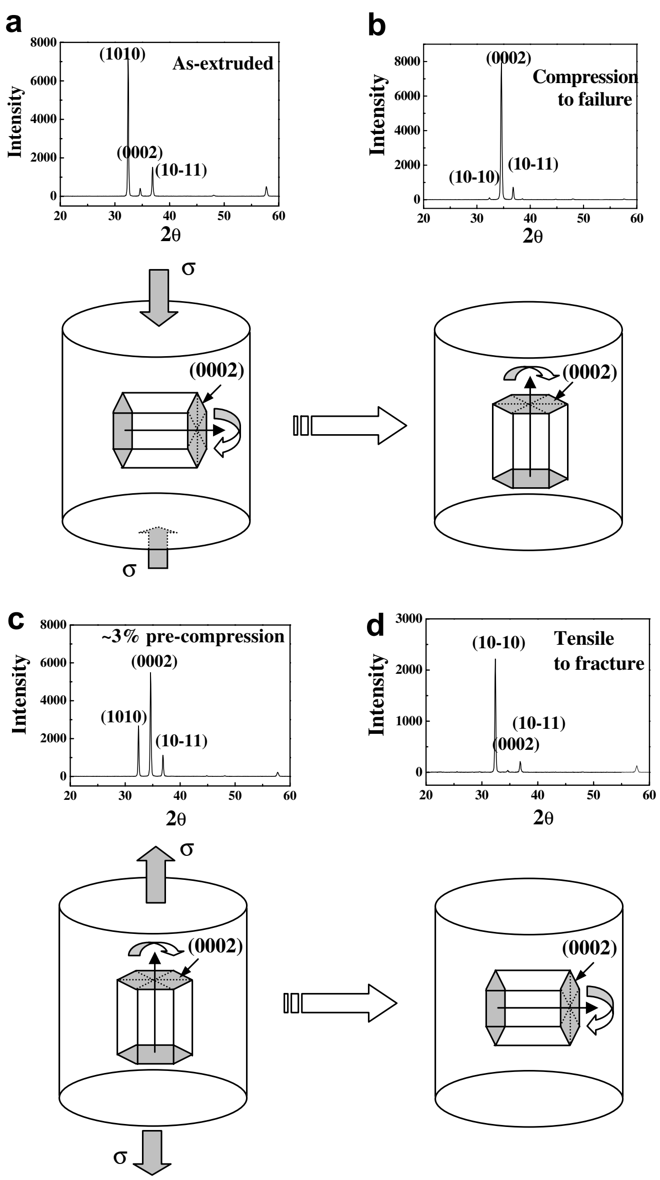

Fig. 12. Schematic drawings showing the change of orientation owing to twinning and untwinning during compression and tension: (a) compression with the stress axis perpendicular to the c-axis; (b) compression causing twinning reorientation to render the c-axis of the twin nearly parallel to the compression axis; (c) tension on the pre-deformed sample with the stress axis parallel to the c-axis; (d) tension causing untwinning reorientation to render the c-axis of the twin nearly perpendicular to the tension axis.

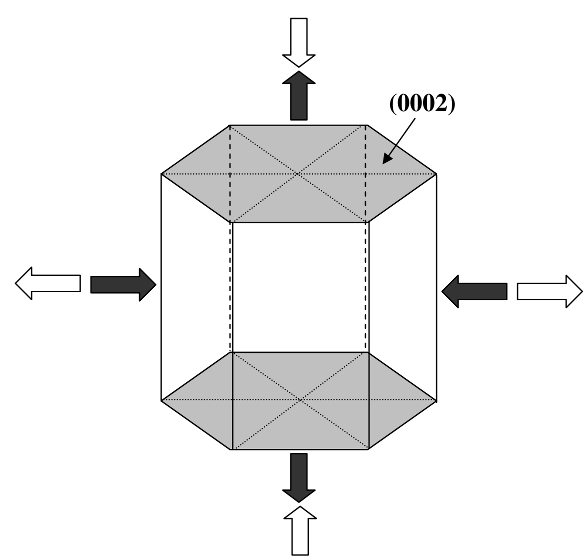

Fig. 13. Schematic diagram showing the relationship between the orientation of favorable $\{10\bar{1}2\}$ twinning and the applied loading directions with respect to the c-axis of hcp-Mg cell ($c/a \approx 1.624$). The black arrows indicate the applied loading directions for favorable twinning; the white arrows indicate the applied loading directions for unfavorable twinning.

nearly the same, at ~160 MPa, irrespective of the amount of pre-deformation strain. This suggests that the tensile yielding is mainly dominated by untwinning. The relationship between the favorable $\{10\bar{1}2\}$ twinning and applied loading directions with respect to the *c*-axis of an hcp cell is illustrated in Fig. 13.

It is well known that there is a grain size strengthening effect, which has not been treated in this paper. From the Hall–Petch equation, the *k*-slope of the current AZ31 alloy under tension has been extracted to be 300 MPa $\mu m^{-1/2}$ [24], or similar to the ~9 MPa $mm^{-1/2}$ previously reported [25]. For the current grain size of 5 μm, the grain size strengthening is around 130 MPa when the operative deformation is basically dislocation slip, as is applicable for the current alloy under tensile testing. The grain size strengthening effect for fine-grain Mg alloys under compression with a dominant twinning operation will be studied more in detail and presented elsewhere.

6. Conclusions

The influence of compressive pre-deformation on the tensile deformation behavior of an extruded AZ31 Mg rod featuring an intense ring fiber texture with the majority of the basal planes laying parallel to the extrusion direction has been investigated. The present hot-extruded rod provided an initial texture, which best favored $\{10\bar{1}2\}$ $\langle 10\bar{1}1\rangle$ twinning under compressive loading. Therefore, this starting texture could activate the twinning at a low degree of deformation, and could result in a comparably low yield stress. Due to the activity of twinning, the *c*-axis of the twin in the compressively deformed samples oriented nearly parallel to the compression axis. These twinned regions are capable of untwinning during reloading of subsequent tension, which results in a significant drop in tensile yield stress, from ~265 to ~160 MPa, irrespective of the amount of pre-strain. All the strains caused by twinning during compressive pre-deformation can be recovered by untwinning during subsequent early tensile deformation, indicating that the tensile yielding is mainly dominated by untwinning.

Acknowledgements

The project was sponsored by National Science Council of Taiwan, ROC (NSC 94-2216-E-110-010 and NSC 94-2811-E-110-004). Y.N.W. is grateful for the sponsorship from Natural Science Foundation of China (50471069).

References

[1] Stohr JF, Poirier JP. Philos Mag 1972;25:1313.
[2] Obara T, Yoshinaga H, Morozumi S. Acta Mater 1973;21:845.
[3] del Valle JA, Perez-Prado MT, Ruano OA. Mater Sci Eng A 2003;355:68.
[4] Mabuchi M, Iwahashi H, Yanase K, Higashi K. Scripta Mater 1996;36:681.
[5] Kim WJ, Hong SI, Kim YS, Min SH, Jeong HT, Lee JD. Acta Mater 2003;51:3293.
[6] Lin HK, Huang JC, Langdon TG. Mater Sci Eng 2005;402:250.
[7] Agnew SR, Mehrotra P, Lillo TM, Stoica GM, Liaw PK. Acta Mater 2005;53:3135.
[8] Wang YN, Huang JC. Mater Trans 2003;44:2276.
[9] Wang YN, Huang JC. Mater Chem Phys 2003;81:11.
[10] Armstrong RW, Zerilli FJ. In: Khan AS, Khoei AR, editors. Proceedings of plastisty '05. Fulton (MD): Neat Press; 2005. p. 172.
[11] Yamashita A, Horita Z, Langdon TG. Mater Sci Eng A 2001;300:142.
[12] Mukai T, Yamanoi M, Watanabe H, Higashi K. Scripta Mater 2001;45:89.
[13] Staroselsky A, Anand L. Int J Plasticity 2003;19:1843.
[14] Agnew SR, Duygulu O. Int J Plasticity 2005;21:1161.
[15] Jiang L, Jonas JJ, Luo AA, Sachdev AK, Godet S. Scripta Mater 2006;54:771.
[16] Nave MD, Barnett MR. Scripta Mater 2004;51:881.
[17] Yi SB, Davies CHJ, Brokmeier HG, Bolmaro RE, Kainer KU, Homeyer J. Acta Mater 2006;54:549.
[18] Hosford WF. The mechanics of crystals and textured polycrystals. Oxford: Oxford University Press; 1993. p. 172.
[19] Christian JW, Mahajan S. Prog Mater Sci 1995;39:1.
[20] Armstrong RW, Horne GT. J Inst Met 1962–63;91:311.
[21] Anken S, Pande CS. Advances in twinning. Warrendale (PA): TMS; 1999. p. 67.
[22] Tenckhoff E. Deformation mechanisms, texture and anisotropy in zirconium and zircoloy. Philadelphia (PA): ASTM; 1988. p. 176.
[23] Gharghouri MA, Weatherly GC, Embury JD, Root J. Philos Mag 1999;79:1671.
[24] Wang YN, Lee CJ, Lin HK, Huang CC, Huang JC. Mater Sci Forum 2003;426–432:2655.
[25] Armstrong RW. Acta Metall 1968;16:347.